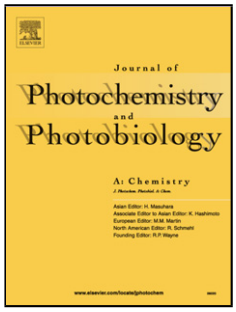

Title: Exploiting Aggregation Induced Emission and Twisted Intramolecular Charge Transfer in a BODIPY Dye for Selective Sensing of Fluoride in Aqueous Medium and Living Cells

Authors: Weilong Che, Guangfu Li, Jianxu Zhang, Yun Geng, Zhigang Xie, Dongxia Zhu, Zhongmin Su

PII: S1010-6030(17)31700-8
DOI: https://doi.org/10.1016/j.jphotochem.2018.03.020
Reference: JPC 11189

To appear in: *Journal of Photochemistry and Photobiology A: Chemistry*

Received date: 21-11-2017
Revised date: 12-3-2018
Accepted date: 13-3-2018

Please cite this article as: Weilong Che, Guangfu Li, Jianxu Zhang, Yun Geng, Zhigang Xie, Dongxia Zhu, Zhongmin Su, Exploiting Aggregation Induced Emission and Twisted Intramolecular Charge Transfer in a BODIPY Dye for Selective Sensing of Fluoride in Aqueous Medium and Living Cells, Journal of Photochemistry and Photobiology A: Chemistry https://doi.org/10.1016/j.jphotochem.2018.03.020

Exploiting Aggregation Induced Emission and Twisted Intramolecular Charge Transfer in a BODIPY Dye for Selective Sensing of Fluoride in Aqueous Medium and Living Cells

Weilong Che [a], Guangfu Li [a], Jianxu Zhang [b], Yun Geng [a], Zhigang Xie [b], Dongxia Zhu [a,*], Zhongmin Su [a,*]

[a] *Key Laboratory of Nanobiosensing and Nanobioanalysis at Universities of Jilin Province, Department of Chemistry, Northeast Normal University, 5268 Renmin Street, Changchun, Jilin Province 130024, P.R. China*

[b] *State key laboratory of Polymer Physics and Chemistry, Changchun Institute of Applied Chemistry Chinese Academy of Sciences, Changchun, 130022, P. R. China*

[*]Corresponding authors

E-mail addresses: zhudx047@nenu.edu.cn (D-X. Zhu.), zmsu@nenu.edu.cn (Z-M. Su.)

Highlights

- A novel BODIPY-based fluorescent probe **TPA-BDP** has been successfully designed and synthesized. The D-A-D structure and twisted molecular conformation make **TPA-BDP** have the AIE and TICT properties simultaneously. This new probe features high sensitivity and excellent selectivity to fluoride with a detection limit of 0.73 μM in aqueous medium. **TPA-BDP** is cell-permeable and can effectively respond to F^- as a suitable fluorescence probe in living cells with very low cytotoxicity.

Abstract

A novel red fluorescent probe based on boron dipyrromethene (BODIPY) was successfully designed

and synthesized, consisting of electron acceptor 1,3,5,7-tetramethyl-8-phenyl-BODIPY (**BDP**) and electron donor triphenylamine (**TPA**) units using Suzuki cross-coupling methods. **TPA-BDP** exploits the advantages of both aggregation-induced emission (AIE) and twisted intramolecular charge transfer (TICT). An X-ray crystal structure of **TPA-BDP** reveals a network of C–H···F intermolecular interactions which can contribute to rigidifying the molecular conformation. Thereby, aggregation restricts the intramolecular rotation associated with the donor moiety, inducing a great enhancement in the emission efficiency. This new dye features high sensitivity and excellent selectivity to fluoride ions with a detection limit of 0.73 μM in aqueous medium. The sensing mechanism was systematically investigated by ^{1}H NMR, ^{19}F NMR, ^{11}B NMR and mass spectrometry. It is proposed that fluoride reacts in a nucleophilic displacement reaction at the **BDP** core which disrupts the structure of **TPA-BDP**, thereby causing the red fluorescence of **TPA-BDP** quenched. It is noteworthy that **TPA-BDP** has been utilized for the fluorescence imaging and fluoride ions detection in living cells with very low cytotoxicity.

Keywords

Aggregation-induced emission; TICT; Fluorescent probe; BODIPY; DFT; Cell image

1. Introduction

Traditional organic luminophores usually emit efficiently in solutions whereas their emission is weakened or even totally quenched upon the formation of molecules aggregates, which facilitate nonradiative pathways and exciton interactions [1-4]. Obviously, aggregation caused quenching (ACQ) is a harmful photophysical effect for light emission and for many practical applications. A very different photophysical property associated with luminophore aggregation is aggregation-induced emission (AIE), first reported by Ben Zhong Tang's group in 2001 [5]. AIE arises as a result of restricted

intramolecular rotations, and is the opposite of ACQ. Since then, AIE materials have attracted considerable attention for potential applications in fields such as the fluorescent detection of ions [6-8]. Recently, various AIE-active materials have been developed for fluorescent sensing [9-13] and bioimaging [14-17]. Previously, we demonstrated an AIE-active ionic iridium complex as a probe for ClO_4^- with high sensitivity and selectivity in bioimaging [18].

Fluoride anions (F^-) play an essential role in human health and fluorescent methods to detect F^- can provide both quantitative and qualitative information [19, 20]. For examples, viable F^- detection has been developed at low energy consumption [21-24], low cost and with the capability for intracellular fluoride detection [25]. It is well known that fluoride has strong affinity toward water. Consequently, few of the reported systems tolerate aqueous conditions [26, 27]. Based on the strong Lewis acid optical chemosensors can be successfully used in water to detect fluoride (e.g., zirconium，lanthanide or organoboron compounds) [28]. And, until now, many fluorescent probes are limited in biosystems due to their ACQ property [29, 30]. Therefore, the development of a fluorescent probe with AIE property to detect F^- in biosystems is an ongoing challenge.

Boron dipyrromethene (BODIPY) dyes are organoboron compounds. It is well-known to be effective in energy-transfer processes, due to their excellent optical properties, such as sharp and intense absorption with relatively long excited-state lifetimes, high fluorescence quantum efficiencies and high molar absorption coefficients [31-34]. Thus, they are frequently used in light-harvesting molecules, as materials for hybrid inorganic/organic LEDs [35] and as probes and labels for biomolecules [36-39]. In 2014, Rurack et al. reported three BODIPY-amidothiourea probes can be used for quantitative detection of inorganic F^- ions in aqueous solution with a remarkable detection limit due to a photoinduced electron-transfer (PET) process [40]. By using this probe, a simple and user-friendly test strip was fabricated that can be applied to determine the F^- ion content in drinking water. Many BODIPY-based dyes emit red light, which is an attractive attribute in the development of efficient bioimaging systems. However, the applications of most BODIPY dyes to living cells are severely restricted due to one or more of the following disadvantages: high background noise, difficulty of preparation, small Stokes

shifts (less than 40 nm), and aggregation-caused quenching (ACQ).

Insert **Scheme 1**

Scheme 1. Synthesis of the target **TPA-BDP** and **Ph-BDP.**

Highly luminescent BODIPY derivatives with AIE performance are rare [41, 42]. Notably, Hu et al. obtained a series of BODIPY derivatives with AIE and twisted intramolecular charge transfer (TICT) properties by introducing an electron donor triphenylamine unit at 8 position [43]. Increasing the "D-A" effect in fluorophores can result in a red shift in their UV-vis absorption and emission spectra, increase the Stokes shift and enlarge the geometrical relaxation [44]. Based on these considerations, we now report a new AIE-active fluorophore containing 1,3,5,7-tetramethyl-8-phenyl-BODIPY (**BDP**) as the electron acceptor (A) and triphenylamine (**TPA**) as the electron donor (D) (**TPA-BDP**, Scheme 1). In our design, we introduced the **TPA** donor to the conventional 1,3,5,7-tetramethyl-8-phenyl-BODIPY at the 2 and 6 positions, to form a symmetrical donor (D)-acceptor (A)-donor (D) structure. This functionalization is clearly distinct from the BODIPY derivatives of Hu et al [43]. Due to the donor (D)-acceptor (A)-donor (D) structure of **TPA-BDP**, it exhibits both AIE and TICT properties. Based on this unusual combination of properties, **TPA-BDP** selectively and sensitively detects F^- among a series of anions. Moreover, **TPA-BDP** is shown to determine F^- in biosystems with very low cytotoxicity.

2. Experimental section

2.1 Materials and instruments

^1H NMR and ^{19}F NMR spectra were recorded at 25 ºC on a Varian 500 MHz spectrometer. Absorption spectra were measured with a Shimadzu UV-3100 spectrophotometer. Photoluminescence spectra were collected on a Shimadzu RF-5301PC spectrophotometer and Maya 2000Pro optical fiber spectrophotometer. PL efficiencies were measured with an integrating sphere (C-701, Labsphere Inc.), with a 365 nm Ocean Optics LLS-LED as the excitation source, and the laser was introduced into the sphere through the optical fiber. Transmission electron microscopy (TEM) of the

sample were performed using a TECNAI F20 microscope. The samples were prepared by placing microdrops of the solution on a holey carbon copper grid. Electrospray ionization and time-of-flight analyzer (ESI-TOF) mass spectra were recorded by both high-resolution electrospray ionization time-of-flight mass spectrometry equipped with high performance liquid chromatography (Agilent 1200HPLC-micrOTOFESI-TOF-MS, and C_{18} columns was applied). Elemental analysis was obtained using a Flash EA1112 analyser. Fluorescence microscopy images were taken on Nikon Eclipse Ti-S inverted fluorescence microscope.

2.2 Synthesis

2.2.1 Synthesis of **TPA-BDP**

1,3,5,7-tetramethyl-8-phenyl-BODIPY (4,4-Difluoro-8-phenyl-1,3,5,7-tetramethyl-4-bora-3a,4a-diaza-s-indacene) and **1** (4,4-Difluoro-8-phenyl-2,6-diiodo-1,3,5,7-tetramethyl-4-bora-3a,4a-diaza-s-indacene) were synthesized by using literature procedures [45-47]. **TPA-BDP** was synthesized from **1** as follows. A mixture of **1** (576 mg, 1.0 mmol), (4-(diphenylamino)phenyl)boronic acid (700 mg, 2.4 mmol) and $Pd(PPh_3)_4$ (60 mg, 0.05 mmol) was dissolved in THF (40 mL) and CH_3OH (10 mL) under nitrogen atmosphere. Aqueous potassium carbonate solution (2 M, 10 mL) was added to the reaction solution and stirred at 80 °C for 24 h. After cooling to room temperature, the reaction mixture was extracted by dichloromethane (3 × 50 mL). The combined organic layer was washed with water and dried over Na_2SO_4. After removal of the solvent, the crude product was purified by column chromatography on silica gel (eluent: ethyl acetate /petroleum ether (1:1, v/v) to obtain **TPA-BDP** (664 mg, 82% yield) as a red solid. ^{1}H NMR (500 MHz, $CDCl_3$), δ (ppm): 7.48 (t, *J* = 8.0 Hz, 3H), 7.36 (d, *J* = 8.0 Hz, 2H), 7.28 (t, *J* = 8.0 Hz, 8H), 7.12 (d, *J* = 7.5 Hz, 8H), 7.07 (d, *J* = 8.5 Hz, 4H), 7.02 (t, *J* = 7.5 Hz, 8H), 2.53 (s, 6H), 1.34 (s, 6H). ^{13}C NMR (125 MHz, $CDCl_3$), δ (ppm): 12.88, 13.49, 123.01, 124.54, 127.43, 128.12, 129.00, 129.22, 129.29, 130.87, 131.35, 135.55, 146.73, 147.66. ESI-MS: Calcd for $C_{55}H_{45}BF_2N_4$ (M^+), m/z 810.37; found 810.33. Anal. Calcd. for $C_{55}H_{45}BF_2N_4$: C 81.48, H 5.59, N 6.91. Found C 81.47,

H 5.57, N 6.94. Crystals for X-ray analysis were grown by slow evaporation of a solution of **TPA-BDP** in a mixture of CH_2Cl_2 and CH_3OH.

2.2.2 Synthesis of **Ph-BDP**

Ph-BDP, was synthesized by using the above procedure except that (4-(diphenylamino)phenyl)boronic acid was replaced by phenylboronic acid. **Ph-BDP** was obtained as a red solid (362 mg, 76% yield). ^{1}H NMR (500 MHz, $CDCl_3$), δ (ppm): 7.50 (t, *J* = 7.5 Hz, 2H), 7.47 (t, *J* = 6.0 Hz, 1H), 7.39 (d, *J* = 6.0 Hz, 3H), 7.36 (d, *J* = 8.5 Hz, 3H), 7.29 (t, *J* = 6.5 Hz, 2H), 7.16 (t, *J* = 7.5 Hz, 4H), 2.54 (s, 6H), 1.31 (s, 6H). ^{13}C NMR (125 MHz, $CDCl_3$), δ (ppm): 12.73, 13.39, 127.07, 128.06, 128.31, 129.04, 129.24, 130.19. ESI-MS: Calcd for $C_{31}H_{27}BF_2N_2$ (M^+), m/z 476.22; found 499.21 $(M+Na)^+$. Anal. Calcd. for $C_{31}H_{27}BF_2N_2$: C 78.16, H 5.71, N 5.88. Found C 78.17, H 5.69, N 5.89.

2.3 X-ray crystallography

For the crystal structure of **TPA-BDP**, the data collection was performed on a Bruker Smart Apex II CCD diffractometer with graphite-monochromated Mo Kα radiation (λ = 0.71069 Å) at room temperature. All absorption corrections were performed by using the SADABS program. The crystal structure was solved by direct methods of SHELXTL-97 [48] and refined by full-matrix least-squares techniques using SHELXTL-97 within WINGX. All hydrogen atoms of the aromatic rings were included in the structure factor calculation at idealized positions by using a riding model. The detailed crystallographic data and structure refinement parameters are summarized in Table S1. Further details of the crystal structure determination have been deposited to the Cambridge Crystallographic Data Centre as supplementary publication. CCDC 1522662 (**TPA-BDP**) contains the supplementary crystallographic data for this paper.

2.4 Theoretical calculations

The electronic structures of the ground states of **TPA-BDP** were investigated by performing density functional theory (DFT) calculations at the B3LYP level. The 6-31G** basis sets were

employed to optimize the C, H and N atoms. All calculations were performed with the D.01 version of the Gaussian 09 program package [49].

2.5 UV-vis and fluorescence (FL) spectra

The stock solution of **TPA-BDP** was prepared in different solvents (10 μM) for solvatochromism experiments. In AIE tests, the stock solution of **TPA-BDP** was prepared in CH_3CN (10 μM) and deionized water was added with different water fractions (0-90 vol%).

For selectivity measurements, all the anions were used as their tetrabutylammonium salts. The test samples were prepared in CH_3CN:H_2O (200 μM, 1:4 v/v). Equal volumes of different anions stock solution were added to **TPA-BDP** solutions (20 μM). The concentrations of the anions were 100 μM for **TPA-BDP**, respectively. Then the absorbance of the solutions of different compositions were recorded. The absorption and fluorescence measurements of the resulting solutions were then performed immediately.

For sensitivity measurements, stock solutions of **TPA-BDP** were prepared in CH_3CN:H_2O (10 μM, 1:4 v/v). The F^- salt was dissolved in CH_3CN:H_2O (1:4 v/v). The titration experiments were carried out by taking 10 μM **TPA-BDP** with the increasing concentration of F^-. The absorption and fluorescence measurements of the resulting solutions were then performed immediately.

For competition measurements, equal concentrations of other anions and F^- were simultaneously added to **TPA-BDP** solutions. The absorption and fluorescence measurements of the resulting solutions were then performed immediately.

For calculation of LOD, the FL intensity (value of the emission maxima) was plotted as a function of F^- concentration for determination of the limit of detection (LOD). LOD values were calculated by standard deviation of the measured value of the emission maxima of a blank solution for eleven times.

2.6 Cell culture

HeLa cells were propagated to confluence in Dulbecco's Modified Eagle Medium (DMEM) supplemented with 100 U mL^{-1} penicillin, 100 μg mL^{-1} streptomycin and 10% FBS, and maintained at 37 ºC in a humidified atmosphere of 5% CO_2 for further cell experiments.

2.7 Cell viability analysis

Cells harvested in a logarithmic growth phase were seeded in 96-well plates at a density of 8×10^3 cells per well and incubated in DMEM for 24 h. The medium was then replaced by 200 μL of DMEM containing predetermined concentrations of **TPA-BDP** (0, 2.5, 5, 12.5, 25, 37.5 and 50 μg mL^{-1}), and then incubated for 24 h, followed by MTT assays to measure the live cells. Cell viabilities were determined by reading the absorbance of the plates at 490 nm with a microplate reader. The cells incubated with DMEM were used as the control. The cell viability (%) =A sample / A control ×100%.

2.8 Cell imaging

Cells harvested in a logarithmic growth phase were seeded in 6-well plates at a density of 2.5×10^5 cells/well and incubated in DMEM for 24 h. The medium was then replaced by DMEM (2 mL) containing **TPA-BDP** (8.1 μg mL^{-1}) and incubated for 1 h at 37 °C. After that, the cells were washed with phosphate buffer saline (PBS) three times and then supplemented with 50 equiv. of F^- (130.5 μg mL^{-1}), Ac^- (159 μg mL^{-1}), Cl^- (139 μg mL^{-1}) and PF_6^- (193.5 μg mL^{-1}) at 37 °C for another 1 h, respectively. Later, the cells were washed with PBS and observed using an inverted fluorescence microscope. The cell samples incubated with only **TPA-BDP** (8.1 μg mL^{-1}), only F^- (130.5 μg mL^{-1}), only Ac^- (159 μg mL^{-1}), only Cl^- (139 μg mL^{-1}) and only PF_6^- (193.5 μg mL^{-1}) were also measured as the controls.

3 Results and discussion

3.1 Synthesis and characterization

The syntheses of target **TPA-BDP** and the model analog **Ph-BDP** are shown in Scheme 1. In the first step, 1,3,5,7-tetramethyl-8-phenyl-BODIPY was synthesized by using literature procedures [45, 46] and

then treated with iodine and iodic acid to produce BDP intermediate **1** [47]. Palladium-mediated Suzuki cross-coupling reaction between **1** and 4-(diphenylamino)phenylboronic acid or 4-phenylboronic acid gave **TPA-BDP** or **Ph-BDP**, respectively. The identity of the products was established by NMR, mass spectra and elemental analysis. Additionally the single-crystal X-ray structure of **TPA-BDP** was obtained (Fig. 1 and Table S1). The torsion angles between the phenyl rings of triphenylamine in **TPA-BDP** are 34.4 °, 44.7°, 49.4°, 30.8°, 44.5° and 57.5° (Fig. 1a). It is shown that three kinds of C–H···F intermolecular interactions exist in the molecular packing of crystalline **TPA-BDP** (Fig. 1b). The network of C–H···F intermolecular interactions is expected to contribute to rigidifying the molecular conformation when the molecule aggregates.

Insert **Fig. 1**

Fig. 1 (a) The molecular structure of **TPA-BDP** in the crystal. The H atoms and solvent molecules are omitted for clarity. (b) The molecular packing in the crystal structure of **TPA-BDP** showing a network of intermolecular C–H···F interactions. (Colour code for heteroatoms: N blue; F green; B brown).

3.2 Photophysical properties

When photoexcited in acetonitrile, 1,3,5,7-tetramethyl-8-phenyl-BODIPY (**BDP**) emits green light (Fig. S5c) with high fluorescence quantum yield (Φ_F = 92%, Scheme 1). The related model compound **Ph-BDP** with phenyl rings at the 2, 6 and 8 positions emits with a much lower fluorescence quantum yield about 50.4% in solution. In marked contrast, under the same conditions **TPA-BDP** emits extremely weak red light with Φ_F = 0.3% as the rotational movement of the phenyl rings of the **TPA** units nonradiatively deactivates its excited state to a large extent [50]. In order to study the electron transfer process of **TPA-BDP**, UV-vis absorption spectra, emission spectra and corresponding excitation spectra of **TPA** and **BDP** have been investigated, respectively (Fig. S5-S6). **TPA** shows a longer fluorescence lifetime (3.54 ns) compared to **BDP** (1.54 ns) and **TPA-BDP** (1.48 ns). Moreover, the overlap between the absorption spectra of **BDP** and the emission spectra of **TPA** indicates the presence of electron transfer process from **TPA** to **BDP** (Fig. S7). The fluorescence emission of **TPA-BDP** in different solvents was also investigated (Fig. 2). Dual emission peaks derived from

locally-excited (LE) and TICT states at 412 nm (Fig. 2, insert) and 598 nm, respectively, were simultaneously observed in a single spectrum in nonpolar hexane solvent upon excitation at 365 nm. Since the dual emission features of **TPA-BDP** in solution was observed, thus, the excitation wavelength corresponding to the short-wavelength emission was selected for photophysical measurement to make sure both emission peaks can be observed (Fig. S8). With increasing solvent polarity, the short-wavelength emission band is nearly no shift, so it is assigned to a LE process from **BDP** (Fig. 2, insert). The long-wavelength emission gradually shifts from λ_{max} 598 to 668 nm and the fluorescence quantum yield decreases dramatically from 47.9% (hexane) to ~0.3% (acetonitrile) (Fig. 2). The color shift with solvent polarity is caused by an intramolecular charge transfer (ICT) process. The value of fluorescence quantum yield should be significantly smaller in polar *vs* nonpolar solvents, since the propensity of TICT state formation is larger in more polar solvents [51]. While electronic excitation generally planarizes the system and thus increases the charge-delocalization interactions, discrepancies have been found for some D-A systems, which undergo torsional motion about the D-A bond and lead to a charge-separated twisted ICT (TICT) state [51]. **TPA-BDP** has a twisted conformation due to the three-bladed propeller-like structure of the triphenylamine units and the twisted conformation will be stabilized in polar solvents, which consequently red-shift the emission spectra. In addition to the bathochromic shift, the emission intensity is decreased as the TICT state is affected by various nonradiative quenching processes [52]. There is precedent that the emission in the TICT state can be modulated by AIE with a simple physical process in aqueous media [43].

Insert **Fig. 2**

Fig. 2 The fluorescence spectra of **TPA-BDP** (10 μM) in different solvents in long-wavelength band at room temperature. Inset: The fluorescence spectra of **TPA-BDP** (10 μM) in different solvents in short-wavelength band at room temperature, excited at 365 nm.

To investigate the AIE property, the fluorescence spectra of **TPA-BDP** in CH_3CN/water mixtures with different fractions of water (f_w) are shown in Fig. 3. **TPA-BDP** is fluorescent in CH_3CN (10 μM) upon excitation at 365 nm. Dual emission peaks derived from LE and TICT states at 412 and 668 nm, respectively. The corresponding absorption spectrum is shown in Fig. S9. **TPA-BDP** in CH_3CN solution displayed three absorption peaks centered at 301, 432 and 541 nm. The data are summarised in Table 1. In polar solvent CH_3CN, the emission around λ_{max} 668 nm of the **TPA-BDP** is from the TICT state that dominates its fluorescence spectra. Addition of large amounts of poor solvents such as water into the solution of the **TPA-BDP** induces the molecules to aggregate, which boosts their TICT emission through the AIE process. The emission intensity at 668 nm increased dramatically with increasing the water content, indicating that **TPA-BDP** is AIE-active (Fig. 3a). However, the fluorescence intensity decreased when the water fraction was higher than 60% (Fig. 3b). This result can be interpreted as the simultaneous formation of crystalline particles and amorphous particles when the f_w > 60% [53]. The emission of **TPA-BDP** in the CH_3CN/water mixture (f_w = 60%) was similar to the solid-state emission of **TPA-BDP** located at λ_{max} 665 nm (Fig. S10). Transmission electron microscopy (TEM) experiments showed that the **TPA-BDP** is uniformly dispersed in the CH_3CN solution, while nanoaggregates are formed in CH_3CN/water mixtures with 60% water fraction (Fig. S11). Thereby, aggregation restricts the intramolecular rotation associated with the donor moiety, inducing a great enhancement in the emission efficiency (Fig. S12).

Insert **Fig. 3**

Fig. 3 (a) The fluorescence spectra of **TPA-BDP** (10 μM) in CH_3CN/water mixtures with different water fractions (0–90% v/v) at room temperature, excited at 365 nm; (b) Emission peak intensity of **TPA-BDP** (10 μM) in CH_3CN/water mixtures with different f_ws.

Insert **Table 1**

Table 1 Detailed photophysical data of **TPA-BDP** in CH_3CN solution (10 μmol).

In contrast, **Ph-BDP** exhibited significant ACQ as expected (Fig. S13). **Ph-BDP** showed strong fluorescence in CH_3CN solution as the methyl groups exert steric hindrance on the rotational motion of the phenyl rings at the 2 and 6 positions, thus effectively reducing the energy loss from nonradiative decay. Its emission intensity is gradually decreased with increasing water content. This confirms that the AIE property of **TPA-BDP** originate from the intramolecular rotation associated with the **TPA** units.

3.3 DFT calculations

To gain further understanding the photophysical and AIE properties, the geometry of **TPA-BDP** was optimized in dilution dichloromethane solution with reference to the X-ray structural data using density functional theory (DFT) methods. The data are given in Tables S2 and S3. Table S2 shows that the major molecular orbitals involved in the main absorption transitions are HOMO-2, HOMO and LUMO, which are exhibited in Fig. S14. The 540 nm absorption band is attributed to electron transfers from the **TPA** to **BDP** unit for S_1 excitation, which is inseparable from the donating and accepting electron ability of **TPA** and **BDP**, respectively. The absorption band at 432 nm shows a $\pi \rightarrow \pi^*$ transition on the **BDP** unit. The corresponding calculated emission data listed in Table S3 indicate the dual emission peaks derived from locally-excited (LE) and TICT states.

According to the Huang-Rhys (HR) factor equation, namely $S_i = (\omega_i D_i^2)/2\hbar$, we calculated the HR factors for **TPA-BDP** (Fig. S15). Since HR factor S_i is calculated in terms of the displacement in the normal mode coordinate D_i, it can characterize the geometrical modification resulting from vibrations when a molecule changes from one electronic state to another, which is important for the internal conversion rate. It is clearly seen from Fig. S15 that most of the large HR factors distribute in the low frequency region, which indicates that molecular rotational vibrations make important contributions to the internal conversion, since rotational vibrations

mostly appear for the low frequency modes. It can be further proved by the vibration analysis of the modes at 114.67 and 127.04 cm^{-1} with the larger HR factors in Fig. S16. It was shown that both the vibrations are mainly derived from the rotational vibration of the three phenyl rings of TPA and the four methyl groups. These rotations are generally easy to restrict by the molecular packing or aggregation, and thus the nonradiative decay is reduced and luminescence is enhanced in the aggregated state.

3.4 Detection of F^-

With its primary AIE property, we investigated the ability of **TPA-BDP** for anion detection in CH_3CN:H_2O (1:4 v/v) (10 μM) at room temperature. The solutions of anions (F^-, Cl^-, Br^-, I^-, Ac^-, HSO_4^-, HPO_4^{2-}, PF_6^-, ClO_4^-, CN^-) were prepared from their tetrabutylammonium salts. Free **TPA-BDP** exhibited high fluorescence intensity in the solution at λ_{max} 668 nm (Fig. 4a). There is no significant change in the emission spectrum for addition of 10 equiv. of other anions except for F^-. It is interesting to observe that the fluorescent intensity significantly decreased at 668 nm in the presence of F^-, which is about 200 times lower than that of the blank solution of **TPA-BDP**. This means that the TICT emission might be disrupted by interaction of **TPA-BDP** specifically with F^-. Its luminescence nearly disappeared in the presence of F^- but showed only little change for other anions, indicating that **TPA-BDP** is highly selective for detecting F^-.

Insert **Fig. 4**

Fig. 4 (a) The fluorescence spectra of **TPA-BDP** (10 μM) in the presence of different anions (1 - blank, 2 - F^-, 3 - Ac^-, 4 - Br^-, 5 - Cl^-, 6 - ClO_4^-, 7 - HPO_4^{2-}, 8 - HSO_4^-, 9 - I^-, 10 - PF_6^-, 11 - CN^-)(10 equiv.) in CH_3CN:H_2O (1:4 v/v), excited at 365 nm. (b) UV-Vis absorption spectra of **TPA-BDP** (10 μM) in the presence of different anions (10 equiv.) in CH_3CN:H_2O (1:4 v/v) solution at room temperature.

To further study the **TPA-BDP** sensing behavior, its absorption spectra changes upon addition of various anions were investigated. The solutions with 10 equiv. of anions (F^-, Cl^-, Br^-, I^-, Ac^-, HSO_4^-, HPO_4^{2-}, PF_6^-, ClO_4^-, CN^-) were added to CH_3CN:H_2O (1:4 v/v) solutions of **TPA-BDP** (10 μM) at

room temperature. Evident changes of the absorption spectrum induced by F^- were observed, whereas the other anions gave only a negligible change in the spectrum (Fig. 4b). Upon addition of F^-, the original absorption band of **TPA-BDP** at 540 nm sharply decreased and slightly red-shifted to 551 nm. The band at 432 nm disappeared, implying new species with less conjugation were formed. This is consistent with the fluorescence spectra (Fig. 4a), further proving that **TPA-BDP** is suitable for selective detection of F^-.

Insert **Fig. 5**

Fig. 5 (a) UV-Vis absorption spectra of **TPA-BDP** (10 μM) upon addition of different amounts of F^- anion (0, 1, 3, 5, 7, 9, 10, 20, 30, 40, 50, 60, 80, 100 μM) in CH_3CN:H_2O (1:4 v/v) solution; (b) The corresponding fluorescence spectra at 668 nm, excited at 365 nm.

In order to evaluate the sensing properties of **TPA-BDP**, UV-vis spectrophotometric titrations were carried out by adding standard solutions of F^- to the CH_3CN:H_2O (1:4 v/v) solutions of **TPA-BDP** (10 μM). With the addition of an increasing concentration of F^-, the absorption band at 540 nm decreased gradually and slightly red-shifted to 551 nm (Fig. 5a). And the F^- sensing property was further investigated through detailed fluorescent titration studies. The emission at 668 nm decreased gradually until nearly disappearing (Fig. 5b), in agreement with the absorption response. These data suggest that the structure of **TPA-BDP** and consequently the TICT emission is disrupted by the addition of F^-.

Insert **Fig. 6**

Fig. 6 Plot of the emission intensity of **TPA-BDP** system in the presence of different anions: **TPA-BDP** (10 μM) + F^- (100 μM) + other anions (100 μM), where other anions = (1 - Ac^-, 2 - Br^-, 3 - Cl^-, 4 - ClO_4^-, 5 - HPO_4^{2-},6 - HSO_4^-, 7 - I^-, 8 - PF_6^-, 9 - CN^-) in CH_3CN:H_2O (1:4 v/v) solution, excited at 365 nm.

It is important to note that **TPA-BDP** retained the sensing response to F^- even in the presence of other anions. **TPA-BDP** in $CH_3CN:H_2O$ (1:4 v/v) solutions (10 μM) were treated with 10 equiv. of F^- in the presence of 10 equiv. of Cl^-, Br^-, I^-, Ac^-, HSO_4^-, HPO_4^{2-}, PF_6^-, ClO_4^-, CN^-. Even in the presence of these anions, the fluorescence intensities of **TPA-BDP** with F^- were quenched immediately (Fig. 6). This indicates that the effect of competitive anions on **TPA-BDP** detection of F^- is slight. This confirms that **TPA-BDP** selectively interacts with F^-, implying that these anions' affinity with **TPA-BDP** are not comparable with F^- in aqueous conditions. The limit of detection (LOD) of F^- is as low as 0.73 μM (0.191 mg/L) which is determined from a plot of normalized fluorescence intensity as a function of the concentration of added F^- (Fig. S19) [54]. This value is much lower than the maximum contaminant level (MCL) defined by the U.S. Environmental Protection Agency (EPA) for fluoride in drinking water (2 mg/L) [55]. Therefore, **TPA-BDP** shows a highly sensitive and selective detection of F^- in the presence of different anions, which is sufficient to detect F^- pollution in Eco-water.

Insert **Scheme 2**

Scheme 2 A possible scheme for the reaction between **TPA-BDP** and F^-.

3.5 Mechanism study

To understand the highly selective fluorescence quenching of **TPA-BDP** upon addition of F^-, ^1H NMR, ^{19}F NMR, ^{11}B NMR and MS analyses were conducted. It seems that nucleophilic displacement favors happening at the hybridized boron center, and fluoride is likely to disrupt the ring by complexing with the central boron atom [56]. So the quenching response of **TPA-BDP** with F^- can be ascribed to nucleophilic displacement of the sp^3 hybridized boron atom in the center of **BDP**, this proposed mechanism is illustrated in Scheme 2. As shown in Fig. 7, a singlet at 7.22 ppm in the ^1H NMR spectrum assigned to the N-H proton was present after

addition of tetrabutylammonium fluoride (TBAF) to **TPA-BDP**. The singlet disappeared on adding one drop of D_2O, consistent with an exchangeable N-H signal. Similarly, there were obvious changes in the ^{19}F NMR spectra upon addition of TBAF (Fig. 8). 1-Iodo-3-(trifluoromethyl)benzene was added as an internal standard. A new peak at −153.50 ppm in the ^{19}F NMR spectra is the same as $[(n\text{-}Bu)_4N]^+BF_4^-$, which proves the formation of the BF_4^- anion in the solution. Furthermore, corresponding ^{11}B NMR spectra was also investigated (Fig. S20). Upon addition of F^- anions, the triplet signal at 1.0 ppm shifted to the 0.8 ppm, which can be assigned to a partially coordinated BF_3 unit [57]. The new singlet peak at -1.0 ppm is corresponding to free BF_4^- anions. Moreover, the negative-ion mass spectrum shows that BF_4^- anions are generated in the solution after the addition of TBAF (Fig. S21). The peak at m/z 810.33 in mass spectrum is correspond to **TPA-BDP** (Fig. S22a). When adding TBAF in the solution, the peak at m/z 810.33 disappears and a new peak at m/z 764.81 appears (Fig. S22b). The new peak corresponds to **TPA-DP**, coming from the damaged structure of **TPA-BDP** by the nucleophilic reaction between F^- and **TPA-BDP**. Furthermore, mass spectrometry experiments and ^1H NMR of **BDP** (**Ph-BDP**) and **BDP** (**Ph-BDP**) with F^- in $CH_3CN/CDCl_3$ have also been performed, as shown in Fig. S23-S26. Mass spectrometry and ^1H NMR results showed that the BF_2 unit bridging two pyrroles are partially detached when added with F^- [57]. The detection of F^- anions cannot be carried out with both **BDP** and **Ph-BDP** compounds due to their native ACQ properties in aqueous media. Therefore, the fluorescence quenching mechanism of **TPA-BDP** response to F^- is identified as: (1) nucleophilic addition of F^-; (2) detachment of the stable difluoroboron bridges; (3) breaking the B-N bond and yielding new B-F and N-H bonds. The D-A-D structure of **TPA-BDP** and the TICT emission are disrupted, resulting in the quenching of the fluorescence of **TPA-BDP** in the presence of F^-.

Insert **Fig. 7**

Fig. 7 ^{1}H NMR spectra of **TPA-BDP**, **TPA-BDP** + TBAF and **TPA-BDP** + TBAF + D_2O in $CDCl_3$.

Insert **Fig. 8**

Fig. 8 ^{19}F NMR spectra of **TPA-BDP** + TBAF, **TPA-BDP,** $[(n\text{-}Bu)_4N]^+BF_4^-$ and TBAF in $CDCl_3$.

3.6 Cellular imaging

The cytotoxicity of **TPA-BDP** was investigated by studying the metabolic viability of HeLa cells after incubation with different concentrations of the **TPA-BDP**. As shown in Fig. 9, no significant change for the cell viability was observed even at a concentration of 50 μg mL^{-1} of **TPA-BDP** after 24 h which indicates that **TPA-BDP** is biocompatible with living cells. This suggests that **TPA-BDP** has a very low cytotoxicity and enables its application as a fluorescent probe for imaging in live cells.

Insert **Fig. 9**

Fig. 9 Cell viabilities of HeLa cells after incubation with different concentrations of **TPA-BDP** (0, 2.5, 5, 12.5, 25, 37.5 and 50 μg mL^{-1}) for 24 h.

The fluorescence imaging of F^- detection using **TPA-BDP** was studied in living cells using scanning confocal microscopy (Fig. 10). Human HeLa cells were incubated with **TPA-BDP** (8.1 μg mL^{-1}) in Dulbecco's Modified Eagle Medium (DMEM) for 1 h at 37 °C. Another sample of HeLa cells was incubated with **TPA-BDP** (8.1 μg mL^{-1}) for 1 h at 37 °C and then supplemented with F^- (130.5 μg mL^{-1}) at 37 °C for another 1 h, and washed with phosphate buffer saline (PBS) to remove the remaining compound. Bright intracellular fluorescence was observed with **TPA-BDP** (Fig. 10a) whereas no intracellular fluorescence can be seen after addition of F^- (Fig.

10c). The marked quenching in intracellular fluorescence suggests that **TPA-BDP** can permeate the cell membrane and respond to the presence of F^- in living cells. As shown in Fig. 10b and 10d, the bright-field measurements suggest that the cells are viable upon treatment with both **TPA-BDP** and F^- throughout the imaging experiments. The contrast experiments were carried out to ensure that only the F^- is responsible for the fluorescence quenching (Fig. S27-S29). After addition of Ac^-, Cl^- and PF_6^- to HeLa cells under the same experimental conditions, no intracellular fluorescence quenching were observed. Thus, these are promising initial proof-of-concept results and **TPA-BDP** has been identified as a potential probe for F^- in living cells.

Insert **Fig. 10**

Fig. 10 (a) Fluorescence and (b) bright-field images of HeLa cells cultured in the presence of **TPA-BDP** (8.1 μg mL^{-1}) in DMEM buffer at 37 ^oC for 1 h; (c) fluorescence and (d) bright-field images of the HeLa cells cultured in the presence of **TPA-BDP** (8.1 μg mL^{-1}) in DMEM buffer at 37 ^oC for 1 h and TBAF (130.5 μg mL^{-1}) in DMEM buffer at 37 ^oC for an additional 1 h. The scale bar is 50 μm.

4. Conclusions

In summary, a novel BODIPY-based probe **TPA-BDP** has been designed and synthesized using triphenylamine and 1,3,5,7-tetramethyl-8-phenyl-BODIPY as the electron donating and accepting units, respectively. The D-A-D structure and twisted molecular conformation endow **TPA-BDP** with both AIE and TICT properties simultaneously, as observed in photophysical experiments and supported by DFT calculations. Obvious fluorescence quenching is observed upon the addition of F^- to the solution of **TPA-BDP** in CH_3CN:H_2O (1:4 v/v). The system shows a high selectivity for detection of F^- with negligible influence from other anions. The very low limit of detection of F^- by **TPA-BDP** [0.73 μM (0.191 mg/L)] indicates that this dye can detect F^- in Eco-water. The fluorescence quenching of **TPA-BDP** can be explained as that a nucleophilic reaction between F^- and **TPA-BDP** at the BF_2 bridges damages the molecular structure and disrupts the TICT emission. Cellular imaging experiments indicate

that **TPA-BDP** has a very low cytotoxicity and could be utilized as a biocompatible fluorescent probe for HeLa cells. From these results we can conclude that specifically functionalized BODIPY derivatives with AIE properties are promising candidates in the development of novel probes for F^- in biosystems.

Acknowledgments

The work was funded by NSFC (No.51473028), the key scientific and technological project of Jilin province (20150204011GX, 20160307016GX), the development and reform commission of Jilin province (20160058). Martin R. Bryce (Durham University, UK) is thanked for helpful discussions.

References

[1] S.M. Borisov, O.S. Wolfbeis, Optical Biosensors, Chem. Rev. 108 (2008) 423-461.

[2] F. Hide, M.A. Díaz-García, B.J. Schwartz, A.J. Heeger, New developments in the photonic applications of conjugated polymers, Acc. Chem. Res. 30 (1997) 430-436.

[3] X. Zhang, D. Görl, V. Stepanenko, F. Wurthner, Hierarchical growth of fluorescent dye aggregates in water by fusion of segmented nanostructures, Angew. Chem. Int. Ed. 53 (2014) 1270-1274.

[4] C. Ma, X. Zhang, L. Yang, Y. Li, H. Liu, Y. Yang, G. Xie, Y.-C. Ou, Y. Wei, Alkyl length dependent mechanofluorochromism of AIE-based phenothiazinyl fluorophenyl acrylonitrile derivatives, Dyes Pigments. 136 (2017) 85-91.

[5] J. Luo, Z. Xie, J.W.Y. Lam, L. Cheng, H. Chen, C. Qiu, H.S. Kwok, X. Zhan, Y. Liu, D. Zhu, B.Z. Tang, Aggregation-induced emission of 1-methyl-1,2,3,4,5-pentaphenylsilole, Chem. Commun. (2001) 1740-1741.

[6] X. Chen, X.Y. Shen, E. Guan, Y. Liu, A. Qin, J.Z. Sun, B.Z. Tang, A pyridinyl-functionalized tetraphenylethylene fluorogen for specific sensing of trivalent cations, Chem. Commun. 49 (2013) 1503-1505.

[7] Y. Hang, J. Wang, T. Jiang, N. Lu, J. Hua, Diketopyrrolopyrrole-based ratiometric/turn-on fluorescent chemosensors for citrate detection in the near-infrared region by an aggregation-induced emission mechanism, Anal. Chem. 88 (2016) 1696-1703.

[8] J. Mei, Y. Hong, J.W. Lam, A. Qin, Y. Tang, B.Z. Tang, Aggregation-induced emission: the whole is more brilliant than the parts, Adv. Mater. 26 (2014) 5429-5479.

[9] X. Dong, F. Hu, Z. Liu, G. Zhang, D. Zhang, A fluorescent turn-on low dose detection of gamma-radiation based on aggregation-induced emission, Chem. Commun. 51 (2015) 3892-3895.

[10] G. Feng, Y. Yuan, H. Fang, R. Zhang, B. Xing, G. Zhang, D. Zhang, B. Liu, A light-up probe with aggregation-induced emission characteristics (AIE) for selective imaging, naked-eye detection and photodynamic killing of Gram-positive bacteria, Chem. Commun. 51 (2015) 12490-12493.

[11] F. Hu, G. Zhang, C. Zhan, W. Zhang, Y. Yan, Y. Zhao, H. Fu, D. Zhang, Highly solid-state emissive pyridinium-substituted tetraphenylethylene salts: emission color-tuning with counter anions and application for optical waveguides, Small. 11 (2015) 1335-1344.

[12] Y. Yuan, R.T. Kwok, B.Z. Tang, B. Liu, Targeted theranostic platinum(IV) prodrug with a built-in aggregation-induced emission light-up apoptosis sensor for noninvasive early evaluation of its therapeutic responses in situ, J. Am. Chem. Soc. 136 (2014) 2546-2554.

[13] J. Liu, Y. Qian, A novel naphthalimide-rhodamine dye: Intramolecular fluorescence resonance energy transfer and ratiometric chemodosimeter for Hg^{2+} and Fe^{3+}, Dyes Pigments. 136 (2017) 782-790.

[14] T. Jiang, Y. Qu, B. Li, Y. Gao, J. Hua, Tetraphenylethene end-capped [1,2,5]thiadiazolo[3,4-c]pyridine with aggregation-induced emission and large two-photon absorption cross-sections, RSC Adv. 5 (2015) 1500-1506.

[15] W. Qin, K. Li, G. Feng, M. Li, Z. Yang, B. Liu, B.Z. Tang, Bright and photostable organic fluorescent dots with aggregation-induced emission characteristics for noninvasive long-term cell imaging, Adv. Funct. Mater. 24 (2014) 635-643.

[16] Y. Yuan, S. Xu, X. Cheng, X. Cai, B. Liu, Bioorthogonal turn-on probe based on aggregation-induced emission characteristics for cancer cell imaging and ablation, Angew. Chem. Int. Ed. 55 (2016) 6457-6461.

[17] L. Bu, J. Chen, X. Wei, X. Li, H. Ågren, Y. Xie, An AIE and ICT based NIR florescent probe for cysteine and homocysteine, Dyes Pigments. 136 (2017) 724-731.

[18] G. Li, W. Guan, S. Du, D. Zhu, G. Shan, X. Zhu, L. Yan, Z. Su, M.R. Bryce, A.P. Monkman, Anion-specific aggregation induced phosphorescence emission (AIPE) in an ionic iridium complex in aqueous media, Chem. Commun. 51 (2015) 16924-16927.

[19] M. Cametti, K. Rissanen, Recognition and sensing of fluoride anion, Chem. Commun. (2009) 2809-2829.

[20] N.H. Evans, P.D. Beer, Advances in anion supramolecular chemistry: from recognition to chemical applications, Angew. Chem. Int. Ed. 53 (2014) 11716-11754.

[21] Y. Bao, B. Liu, H. Wang, J. Tian, R. Bai, A "naked eye" and ratiometric fluorescent chemosensor for rapid detection of F^- based on combination of desilylation reaction and excited-state proton transfer, Chem. Commun. 47 (2011) 3957-3959.

[22] R. Hu, J. Feng, D. Hu, S. Wang, S. Li, Y. Li, G. Yang, A rapid aqueous fluoride ion sensor with dual output modes, Angew. Chem. Int. Ed. 49 (2010) 4915-4918.

[23] Q. Zhao, F. Li, S. Liu, M. Yu, Z. Liu, T. Yi, C. Huang, Highly selective phosphorescent chemosensor for fluoride based on an iridium(ш) complex containing arylborane units, Inorg. Chem. 47 (2008) 9256-9264.

[24] A. Mohammadi, Z. Dehghan, M. Rassa, N. Chaibakhsh, Colorimetric probes based on bioactive organic dyes for selective sensing of cyanide and fluoride ions, Sens. Actuators B. 230 (2016) 388-397.

[25] Q. Diao, P. Ma, L. Lv, T. Li, Y. Sun, X. Wang, D. Song, A water-soluble and reversible fluorescent probe for Al^{3+} and F^- in living cells, Sens. Actuators B. 229 (2016) 138-144.

[26] S. Guha, S. Saha, Fluoride ion sensing by an anion-π interaction, J. Am. Chem. Soc. 132 (2010) 17674-17677.

[27] F. Wang, J. Wu, X. Zhuang, W. Zhang, W. Liu, P. Wang, S. Wu, A highly selective fluorescent sensor for fluoride in aqueous solution based on the inhibition of excited-state intramolecular proton transfer, Sens. Actuators B. 146 (2010) 260-265.

[28] S. Rochat, K. Severin, A simple fluorescence assay for the detection of fluoride in water at neutral pH, Chem. Commun. 47 (2011) 4391-4393.

[29] O.A. Bozdemir., F. Sozmen., O. Buyukcakir., R. Guliyev., Y. Cakmak., E.U. Akkaya, Reaction-based sensing of fluoride ions using built-in triggers for intramolecular charge transfer and photoinduced electron transfer, Org. Lett. 12 (2010) 1400-1403.

[30] S. Madhu, M. Ravikanth, Boron-dipyrromethene based reversible and reusable selective chemosensor for fluoride detection, Inorg. Chem. 53 (2014) 1646-1653.

[31] X.-D. Jiang, J. Guan, J. Zhao, B. Le Guennic, D. Jacquemin, Z. Zhang, S. Chen, L. Xiao, Synthesis, structure and photophysical properties of NIR aza-BODIPYs with $F/N_3/NH_2$ groups at 1,7-positions, Dyes Pigments. 136 (2017) 619-626.

[32] K.G. Thorat, A.K. Ray, N. Sekar, Modulating TICT to ICT characteristics of acid switchable red emitting boradiazaindacene chromophores: Perspectives from synthesis, photophysical, hyperpolarizability and TD-DFT studies, Dyes Pigments. 136 (2017) 321-334.

[33] H.-B. Sun, S.-J. Liu, T.-C. Ma, N.-N. Song, Q. Zhao, W. Huang, An excellent BODIPY dye containing a benzo[2,1,3]thiadiazole bridge as a highly selective colorimetric and fluorescent probe for Hg^{2+} with naked-eye detection, New. J. Chem. 35 (2011) 1194-1197.

[34] D. Bai, A.C. Benniston, J. Hagon, H. Lemmetyinen, N.V. Tkachenko, R.W. Harrington, Tuning the förster overlap integral: energy transfer over 20 Ångstroms from a pyrene-based donor to borondipyrromethene (Bodipy), Phys. Chem. Chem. Phys. 15 (2013) 9854-9861.

[35] E. Taylor-Shaw, E. Angioni, N.J. Findlay, B. Breig, A.R. Inigo, J. Bruckbauer, D.J. Wallis, P.J. Skabara, R.W. Martin, Cool to warm white light emission from hybrid inorganic/organic light-emitting diodes, J. Mater. Chem. C. 4 (2016) 11499-11507.

[36] E.V. Antina, N.A. Bumagina, A.I. V'yugin, A.V. Solomonov, Fluorescent indicators of metal ions based on dipyrromethene platform, Dyes Pigments. 136 (2017) 368-381.

[37] B.L. Watson, T.A. Moore, A.L. Moore, D. Gust, Synthesis of a novel building block for the preparation of multi-chromophoric sensitizers for panchromatic dye-sensitized solar cells, Dyes Pigments. 136 (2017) 893-897.

[38] A.B. Nepomnyashchii, M. Broring, J. Ahrens, A.J. Bard, Synthesis, photophysical, electrochemical, and electrogenerated chemiluminescence studies. Multiple sequential electron transfers in BODIPY monomers, dimers, trimers, and polymer, J. Am. Chem. Soc. 133 (2011) 8633-8645.

[39] L. Wu, Aurore Loudet, R. Barhoumi, R.C. Burghardt, K. Burgess, Fluorescent cassettes for monitoring three-component interactions *in vitro* and in living cells, J. Am. Chem. Soc. 131 (2009) 9156-9157.

[40] P. Ashokkumar, H. Weisshoff, W. Kraus, K. Rurack, Test-strip-based fluorometric detection of fluoride in aqueous media with a BODIPY-linked hydrogen-bonding receptor, Angew. Chem. Int. Ed. 53 (2014) 2225-2229.

[41] Z. Li, M. Zheng, X. Guan, Z. Xie, Y. Huang, X. Jing, Unadulterated BODIPY-dimer nanoparticles with high stability and good biocompatibility for cellular imaging, Nanoscale. 6 (2014) 5662-5665.

[42] Z. Zhao, B. Chen, J. Geng, Z. Chang, L. Aparicio-Ixta, H. Nie, C.C. Goh, L.G. Ng, A. Qin, G. Ramos-Ortiz, B. Liu, B.Z. Tang, Red emissive biocompatible nanoparticles from tetraphenylethene-decorated BODIPY luminogens for two-photon excited fluorescence cellular imaging and mouse brain blood vascular visualization, Part. Part. Syst. Char. 31 (2014) 481-491.

[43] R. Hu, E. Lager, A. Aguilar-Aguilar, J. Liu, J.W.Y. Lam, H.H.Y. Sung, I.D. Williams, Y. Zhong, K.S. Wong, E. Peña-Cabrera, B.Z. Tang, Twisted intramolecular charge transfer and aggregation-induced emission of BODIPY derivatives, J. Phys. Chem. C. 113 (2009) 15845–15853.

[44] M. Jiang, X. Gu, J.W.Y. Lam, Y. Zhang, R.T.K. Kwok, K.S. Wong, B.Z. Tang, Two-photon AIE bio-probe with large Stokes shift for specific imaging of lipid droplets, Chem. Sci. 8 (2017) 5440-5446.

[45] M. Emrullahoğlu, M. Üçüncü, E. Karakuş, A BODIPY aldoxime-based chemodosimeter for highly selective and rapid detection of hypochlorous acid, Chem. Commun. 49 (2013) 7836-7838.

[46] M. Isik, T. Ozdemir, I.S. Turan, S. Kolemen, E.U. Akkaya, Chromogenic and fluorogenic sensing of biological thiols in aqueous solutions using BODIPY-based reagents, Org. Lett. 15 (2013) 216-219.

[47] Y. Wu, X. Ma, J. Jiao, Y. Cheng, C. Zhu, Synthesis and characterization of near-infrared emissive BODIPY-based conjugated polymers, Synlett. 23 (2012) 778-782.

[48] Sheldrick GM, SHELXL-97, program for crystal structure refinement. University of Göttingen; 1997.

[49] Frisch MJ, Trucks GW, Schlegel HB, Scuseria GE, Robb MA, Cheeseman JR, et al. Gaussian 09W, revision A.02. Wallingford CT: Gaussian, Inc.; 2009.

[50] A. Loudet, K. Burgess, BODIPY Dyes and their derivatives: syntheses and spectroscopic properties, Chem. Rev. 107 (2007) 4891-4932.

[51] J.-S. Yang, K.-L. Liau, C.-Y. Li, M.-Y. Chen, Meta conjugation effect on the torsional motion of aminostilbenes in the photoinduced intramolecular charge-transfer state, J. Am. Chem. Soc. 129 (2007) 13183-13192.

[52] L. Hu, J. Sun, J. Han, Y. Duan, T. Han, An AIE luminogen as a multi-channel sensor for ethanol, Sens. Actuators B. 239 (2017) 467-473.

[53] Y. Jiang, G. Li, W. Che, Y. Liu, B. Xu, G. Shan, D. Zhu, Z. Su, M.R. Bryce, A neutral dinuclear Ir(ш) complex for anti-counterfeiting and data encryption, Chem. Commun. 53 (2017) 3022-3025.

[54] W. Che, T. Yu, D. Jin, X. Ren, D. Zhu, Z. Su, M.R. Bryce, A simple oxazoline as fluorescent sensor for Zn^{2+} in aqueous media, Inorg. Chem. Commun. 69 (2016) 89-93.

[55]https://www.epa.gov/dwregdev/drinking-water-regulations-and-contaminants#Secondary

[56] L. Wang, G. Fang, D. Cao, Highly selective and sensitive detection of F^- and CN^- ions simultaneously by a reaction-based BODIPY-containing conjugated polymer, Sens. Actuators B. 221 (2015) 63-74.

[57] R. Guliyev, S. Ozturk, E. Sahin, E. U. Akkaya, Expanded bodipy dyes: anion sensing using a bodipy analog with an additional difluoroboron bridge, Org. Lett. 14 (2012) 1528-1531.

Figure Captions

Scheme 1. Synthesis of the target **TPA-BDP** and **Ph-BDP**.

Fig. 1 (a) The molecular structure of **TPA-BDP** in the crystal. The H atoms and solvent molecules are omitted for clarity. (b) The molecular packing in the crystal structure of **TPA-BDP** showing a network of intermolecular C–H···F interactions. (Colour code for heteroatoms: N blue; F green; B brown).

Fig. 2 The fluorescence spectra of **TPA-BDP** (10 μM) in different solvents in long-wavelength band at room temperature. Inset: The fluorescence spectra of **TPA-BDP** (10 μM) in different solvents in short-wavelength band at room temperature, excited at 365 nm.

Fig. 3 (a) The fluorescence spectra of **TPA-BDP** (10 μM) in CH_3CN/water mixtures with different water fractions (0–90% v/v) at room temperature, excited at 365 nm; (b) Emission peak intensity of **TPA-BDP** (10 μM) in CH_3CN/water mixtures with different f_ws.

Table 1 Detailed photophysical data of **TPA-BDP** in CH_3CN solution (10 μmol).

Fig. 4 (a) The fluorescence spectra of **TPA-BDP** (10 μM) in the presence of different anions (1 - blank, 2 - F^-, 3 - Ac^-, 4 - Br^-, 5 - Cl^-, 6 - ClO_4^-, 7 - HPO_4^{2-}, 8 - HSO_4^-, 9 - I^-, 10 - PF_6^-, 11 - CN^-)(10 equiv.) in CH_3CN:H_2O (1:4 v/v), excited at 365 nm. (b) UV-Vis absorption spectra of **TPA-BDP** (10 μM) in the presence of different anions (10 equiv.) in CH_3CN:H_2O (1:4 v/v) solution at room temperature.

Fig. 5 (a) UV-Vis absorption spectra of **TPA-BDP** (10 μM) upon addition of different amounts of F^- anion (0, 1, 3, 5, 7, 9, 10, 20, 30, 40, 50, 60, 80, 100 μM) in CH_3CN:H_2O (1:4 v/v) solution; (b) The corresponding fluorescence spectra at 668 nm, excited at 365 nm.

Fig. 6 Plot of the emission intensity of **TPA-BDP** system in the presence of different anions: **TPA-BDP** (10 μM) + F^- (100 μM) + other anions (100 μM), where other anions = (1 - Ac^-, 2 - Br^-, 3 - Cl^-, 4 -

ClO_4^-, 5 - HPO_4^{2-},6 - HSO_4^-, 7 - I^-, 8 - PF_6^-, 9 - CN^-) in CH_3CN:H_2O (1:4 v/v) solution, excited at 365 nm.

Scheme 2. A possible scheme for the reaction between **TPA-BDP** and F^-.

Fig. 7 ^1H NMR spectra of **TPA-BDP**, **TPA-BDP** + TBAF and **TPA-BDP** + TBAF + D_2O in $CDCl_3$.

Fig. 8 ^{19}F NMR spectra of **TPA-BDP** + TBAF, **TPA-BDP**, $[(n\text{-}Bu)_4N]^+BF_4^-$ and TBAF in $CDCl_3$.

Fig. 9 Cell viabilities of HeLa cells after incubation with different concentrations of **TPA-BDP** (0, 2.5, 5, 12.5, 25, 37.5 and 50 μg mL^{-1}) for 24 h.

Fig. 10 (a) Fluorescence and (b) bright-field images of HeLa cells cultured in the presence of **TPA-BDP** (8.1 μg mL^{-1}) in DMEM buffer at 37 ºC for 1 h; (c) fluorescence and (d) bright-field images of the HeLa cells cultured in the presence of **TPA-BDP** (8.1 μg mL^{-1}) in DMEM buffer at 37 ºC for 1 h and TBAF (130.5 μg mL^{-1}) in DMEM buffer at 37 ºC for an additional 1 h. The scale bar is 50 μm.

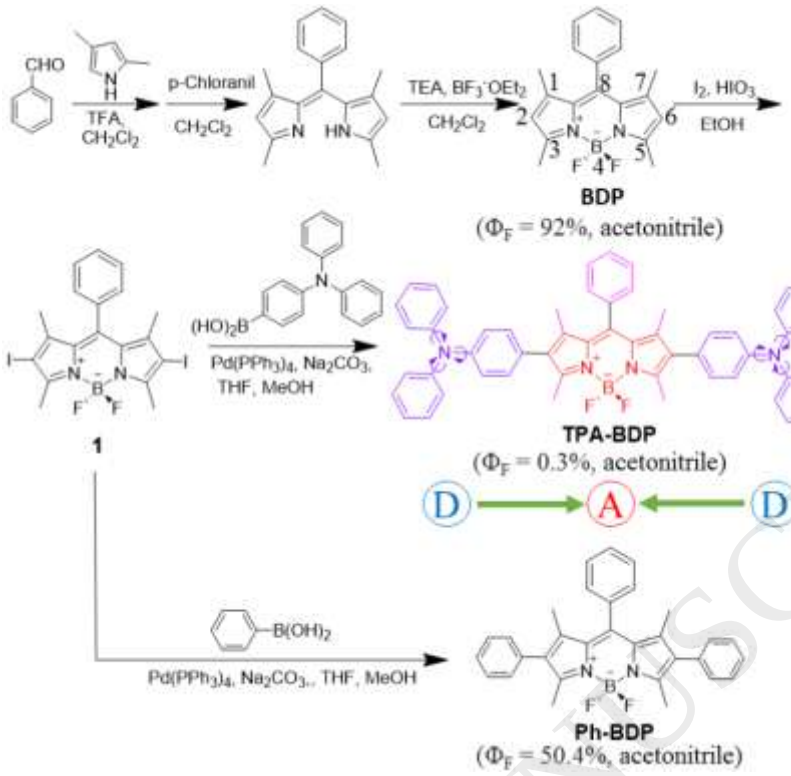

Scheme 1. Synthesis of the target **TPA-BDP** and **Ph-BDP**.

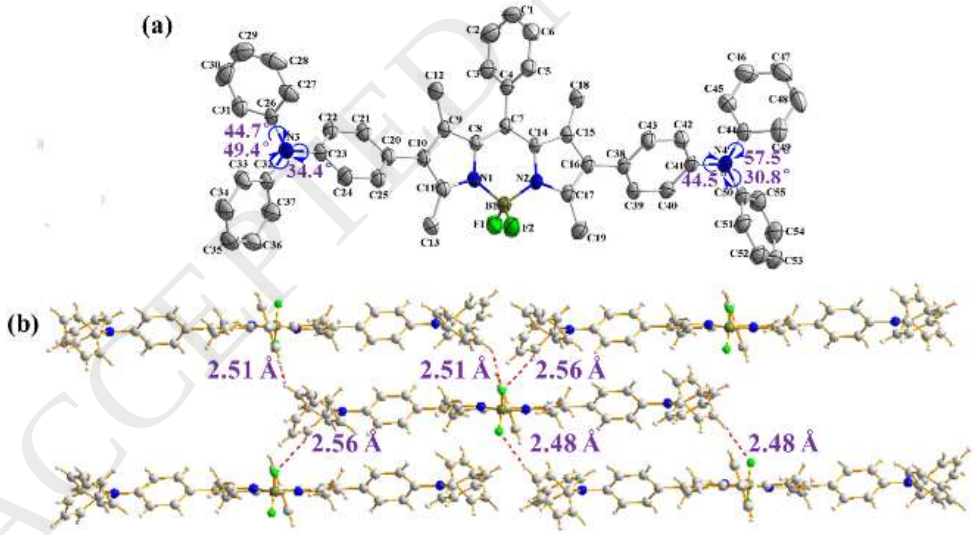

Fig. 1 (a) The molecular structure of **TPA-BDP** in the crystal. The H atoms and solvent molecules are omitted for clarity. (b) The molecular packing in the crystal structure of **TPA-BDP** shows a network of intermolecular C–H···F interactions. (Colour code for heteroatoms: N blue; F green; B brown).

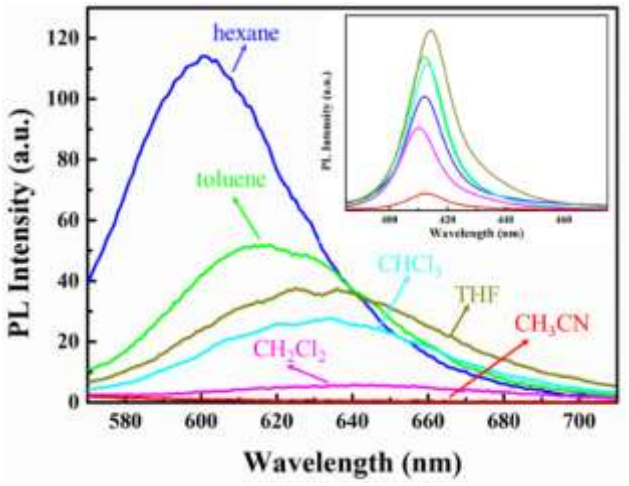

Fig. 2 The fluorescence spectra of **TPA-BDP** (10 μM) in different solvents in long-wavelength band at room temperature. Inset: The fluorescence spectra of **TPA-BDP** (10 μM) in different solvents in short-wavelength band at room temperature, excited at 365 nm.

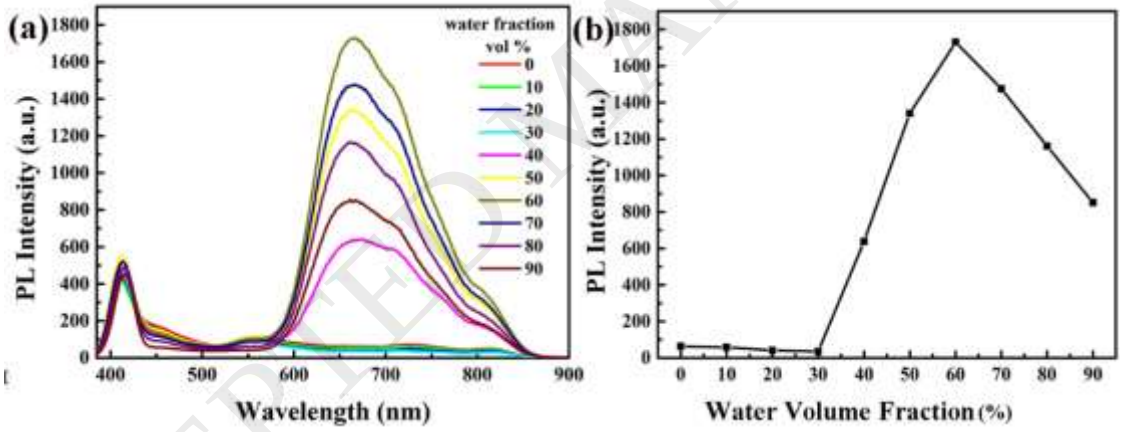

Fig. 3 (a) The fluorescence spectra of **TPA-BDP** (10 μM) in CH_3CN/water mixtures with different water fractions (0–90% v/v) at room temperature, excited at 365 nm; (b) Emission peak intensity of **TPA-BDP** (10 μM) in CH_3CN/water mixtures with different f_ws.

Table 1 Detailed photophysical data of **TPA-BDP** in CH_3CN solution (10 μmol).

	λ_{abs} (nm)	λ_{em} (nm)	Φ_F (%)	τ (ns)	k_r ($\times 10^7$ s^{-1})	k_{nr} ($\times 10^7$ s^{-1})
TPA-BDP	301, 432, 541	412, 668	2.4, 0.3	1.45, 1.48	1.66, 0.20	67.31, 63.36

The radiative k_r and non-radiative k_{nr} values in neat film were calculated according to the equations: $k_r = \Phi/\tau$ and $k_{nr} = (1 - \Phi)/\tau$, from the quantum yields Φ_F and the lifetime τ values.

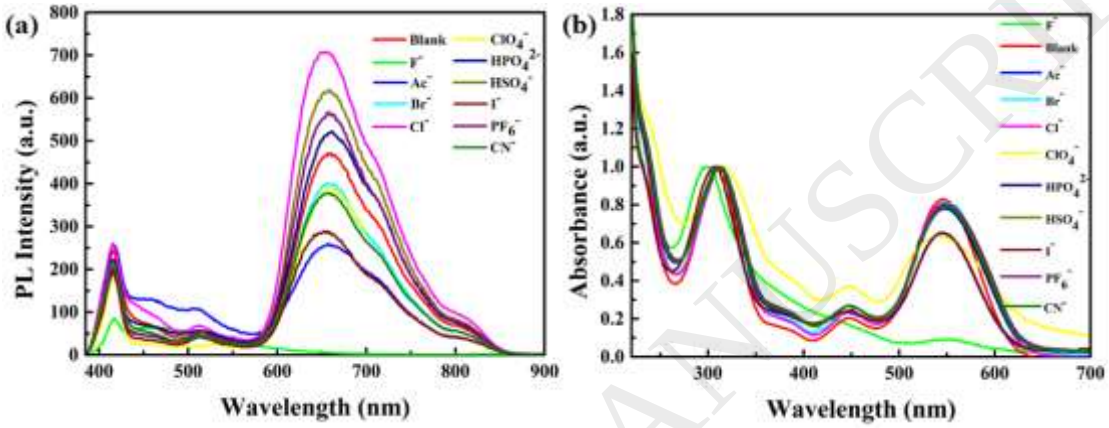

Fig. 4 (a) The fluorescence spectra of **TPA-BDP** (10 μM) in the presence of different anions (1 - blank, 2 - F^-, 3 - Ac^-, 4 - Br^-, 5 - Cl^-, 6 - ClO_4^-, 7 - HPO_4^{2-}, 8 - HSO_4^-, 9 - I^-, 10 - PF_6^-, 11 - CN^-)(10 equiv.) in CH_3CN:H_2O (1:4 v/v), excited at 365 nm. (b) UV-Vis absorption spectra of **TPA-BDP** (10 μM) in the presence of different anions (10 equiv.) in CH_3CN:H_2O (1:4 v/v) solution at room temperature.

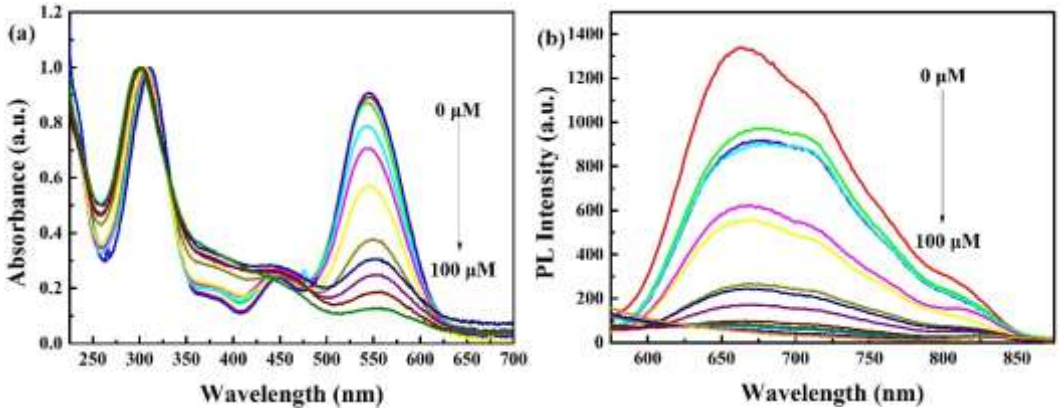

Fig. 5 (a) UV-Vis absorption spectra of **TPA-BDP** (10 μM) upon addition of different amounts of F^- anion (0, 1, 3, 5, 7, 9, 10, 20, 30, 40, 50, 60, 80, 100 μM) in $CH_3CN:H_2O$ (1:4 v/v) solution; (b) The corresponding fluorescence spectra at 668 nm, excited at 365 nm.

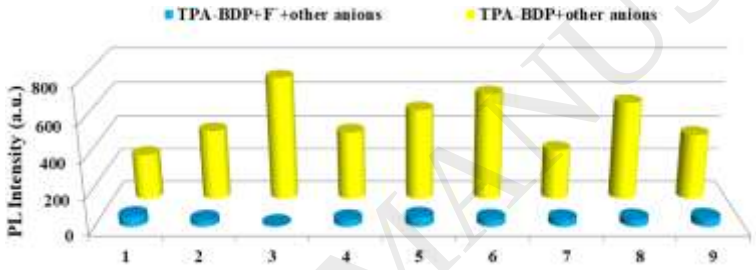

Fig. 6 Plot of the emission intensity of **TPA-BDP** system in the presence of different anions: **TPA-BDP** (10 μM) + F^- (100 μM) + other anions (100 μM), where other anions = (1 - Ac^-, 2 - Br^-, 3 - Cl^-, 4 - ClO_4^-, 5 - HPO_4^{2-},6 - HSO_4^-, 7 - I^-, 8 - PF_6^-, 9 - CN^-) in $CH_3CN:H_2O$ (1:4 v/v) solution, excited at 365 nm.

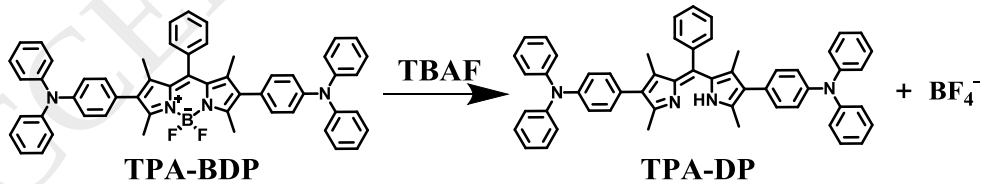

Scheme 2. A possible scheme for the reaction between **TPA-BDP** and F^-.

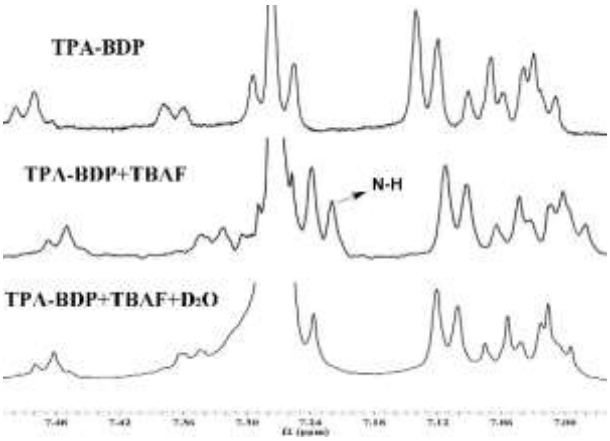

Fig. 7 ^{1}H NMR spectra of **TPA-BDP**, **TPA-BDP** + TBAF and **TPA-BDP** + TBAF + D_2O in $CDCl_3$.

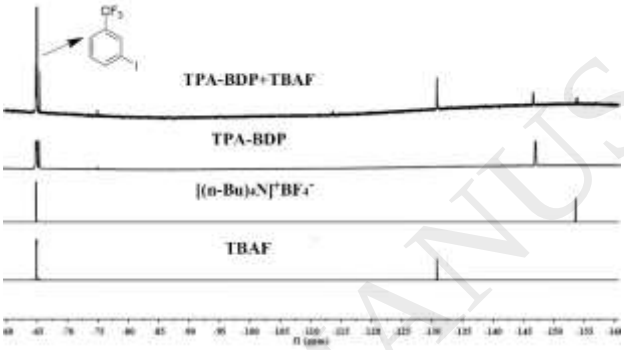

Fig. 8 ^{19}F NMR spectra of **TPA-BDP** + TBAF, **TPA-BDP**, $[(n\text{-}Bu)_4N]^+BF_4^-$ and TBAF in $CDCl_3$.

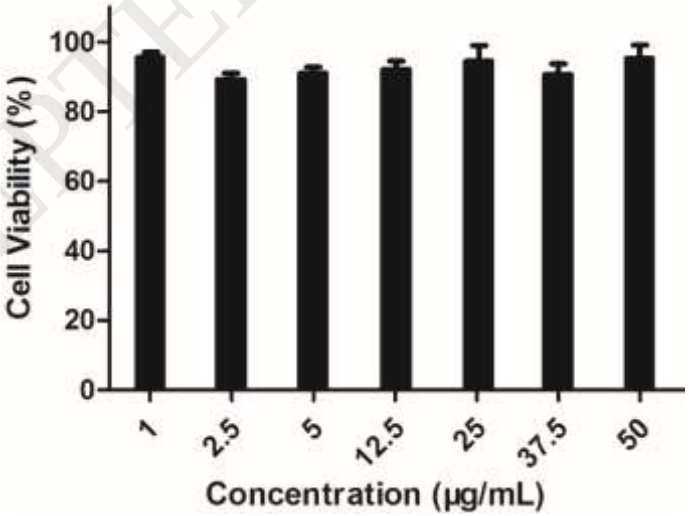

Fig. 9 Cell viabilities of HeLa cells after incubation with different concentrations of **TPA-BDP** (0, 2.5, 5, 12.5, 25, 37.5 and 50 μg mL^{-1}) for 24 h.

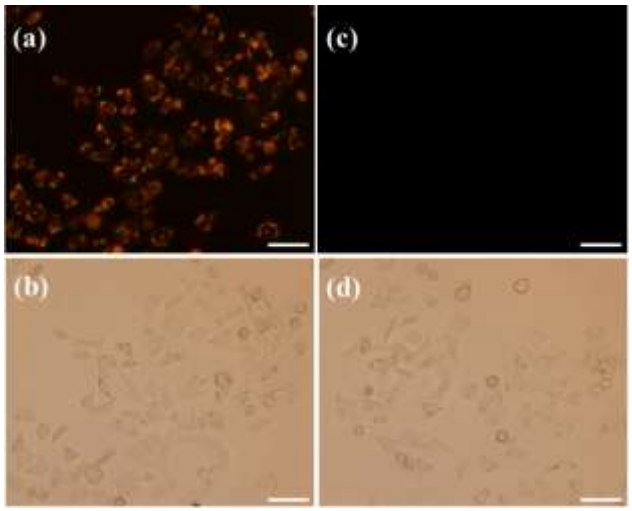

Fig. 10 (a) Fluorescence and (b) bright-field images of HeLa cells cultured in the presence of **TPA-BDP** (8.1 μg mL^{-1}) in DMEM buffer at 37 ºC for 1 h; (c) fluorescence and (d) bright-field images of the HeLa cells cultured in the presence of **TPA-BDP** (8.1 μg mL^{-1}) in DMEM buffer at 37 ºC for 1 h and TBAF (130.5 μg mL^{-1}) in DMEM buffer at 37 ºC for an additional 1 h. The scale bar is 50 μm.